LETTER

Rapid cycling of reactive nitrogen in the marine boundary layer

Chunxiang Ye[1], Xianliang Zhou[1,2], Dennis Pu[2], Jochen Stutz[3], James Festa[3], Max Spolaor[3], Catalina Tsai[3], Christopher Cantrell[4], Roy L. Mauldin III[4,5], Teresa Campos[6], Andrew Weinheimer[6], Rebecca S. Hornbrook[6], Eric C. Apel[6], Alex Guenther[7], Lisa Kaser[6], Bin Yuan[8,9], Thomas Karl[10], Julie Haggerty[6], Samuel Hall[6], Kirk Ullmann[6], James N. Smith[6,11], John Ortega[6] & Christoph Knote[6]†

Nitrogen oxides are essential for the formation of secondary atmospheric aerosols and of atmospheric oxidants such as ozone and the hydroxyl radical, which controls the self-cleansing capacity of the atmosphere[1]. Nitric acid, a major oxidation product of nitrogen oxides, has traditionally been considered to be a permanent sink of nitrogen oxides[1]. However, model studies predict higher ratios of nitric acid to nitrogen oxides in the troposphere than are observed[2,3]. A 'renoxification' process that recycles nitric acid into nitrogen oxides has been proposed to reconcile observations with model studies[2–4], but the mechanisms responsible for this process remain uncertain[5–9]. Here we present data from an aircraft measurement campaign over the North Atlantic Ocean and find evidence for rapid recycling of nitric acid to nitrous acid and nitrogen oxides in the clean marine boundary layer via particulate nitrate photolysis. Laboratory experiments further demonstrate the photolysis of particulate nitrate collected on filters at a rate more than two orders of magnitude greater than that of gaseous nitric acid, with nitrous acid as the main product. Box model calculations based on the Master Chemical Mechanism[10,11] suggest that particulate nitrate photolysis mainly sustains the observed levels of nitrous acid and nitrogen oxides at midday under typical marine boundary layer conditions. Given that oceans account for more than 70 per cent of Earth's surface, we propose that particulate nitrate photolysis could be a substantial tropospheric nitrogen oxide source. Recycling of nitrogen oxides in remote oceanic regions with minimal direct nitrogen oxide emissions could increase the formation of tropospheric oxidants and secondary atmospheric aerosols on a global scale.

Nitrogen oxides ($NO_x = NO$ and NO_2) are essential in the formation of secondary aerosol and atmospheric oxidants, such as ozone (O_3) and hydroxyl radicals (OH)[1]. Nitric acid (HNO_3) is a major oxidation product of NO_x. The formation of HNO_3 has traditionally been considered to be a permanent sink of NO_x owing to the small photolysis frequency of gaseous HNO_3 and to its rapid removal from the troposphere by wet and dry deposition[1]. However, this traditional view has recently been challenged by laboratory studies demonstrating that photolysis of surface-adsorbed HNO_3 is enhanced by one to four orders of magnitude, compared to gaseous HNO_3 and aqueous nitrate, with NO_x and nitrous acid ($HONO$) as products[5–8]. Field observations have provided further evidence that photolysis of HNO_3 adsorbed on the forest canopy surfaces is the primary daytime $HONO$ source for the overlying atmosphere[9]. Model simulations that include $HONO$ observations or photolytic $HONO$ formation mechanisms have substantially improved estimates of atmospheric oxidant formation[12,13].

However, it remains unknown whether photolysis of particulate nitrate (pNO_3) contributes to the $HONO$ and NO_x budgets and affects the formation of oxidants and secondary aerosol.

The Nitrogen, Oxidants, Mercury and Aerosol Distributions, Sources and Sinks (NOMADSS) field study was conducted in the summer of 2013 aboard the NSF/NCAR C-130 aircraft. One objective was to investigate the role of pNO_3 photolysis in reactive nitrogen cycling. Two research flights in particular, RF14 on 5 July 2013 and RF16 on 8 July 2013, involved similar flight tracks in the marine boundary layer (MBL) and the free troposphere over the North Atlantic Ocean (flight tracks from 33° 39′ N, 77° 42′ W to 32° 11′ N, 77° 41′ W). The flight periods in the MBL and the free troposphere over the Atlantic Ocean took place between 12:00 and 15:00 Eastern Standard Time (equivalent to Coordinated Universal Time (UTC) minus 5 h). The solar elevation angle during the flight legs in the MBL for both research flights was between 17° and 31°. A comprehensive suite of parameters relevant to the research objective were simultaneously measured, including $HONO$, NO_x, pNO_3, HNO_3, aerosol surface area density (for particle diameters $<1\,\mu m$), OH, hydroperoxyl (HO_2) and alkylperoxyl (RO_2) radicals, bromine oxide (BrO), iodine oxide (IO), O_3, volatile organic compounds (VOCs), and photolysis frequencies J (see Extended Data Table 1). The air masses encountered in the MBL consisted mostly of aged marine air circulating over the North Atlantic Ocean under a Bermuda high-pressure system as indicated by back-trajectories, with slight influence from coastal emissions in RF16 (Extended Data Fig. 1).

The observed mixing ratios of $HONO$, NO_x and pNO_3 versus altitude are shown in Fig. 1. The mixing ratios of NO_x ranged from 10 to 40 parts per trillion by volume (p.p.t.v.), and were comparable to previous observations in the clean MBL[14]. The mean mixing ratios of $HONO$ (± 1 s.d., standard deviation) within the MBL were 11.3 ± 1.6 p.p.t.v. for RF14 and 8.8 ± 2.3 p.p.t.v. for RF16. These $HONO$ values are substantially lower than other airborne observations in the continental boundary layer over Northern Michigan (8–70 p.p.t.v.)[15] and in the morning residual layer over an industrial region of Northern Italy (up to 150 p.p.t.v.)[16]. These low $HONO$ values are consistent with the lower levels of its precursors, such as NO_x, in this clean MBL compared to the other two locations. In addition, the ocean surface is likely to be a net $HONO$ sink given the slight alkalinity of sea water, while the land surface is typically a net $HONO$ source for the overlying atmosphere[9,15].

The photolysis lifetime of $HONO$ during the flight legs discussed here was approximately 12 min. To balance the photolytic loss and maintain a nearly steady-state $HONO$ concentration, there must be an *in situ* $HONO$ source well distributed in the MBL. NO_x is a well

[1]Wadsworth Center, New York State Department of Health, Albany, New York, USA. [2]Department of Environmental Health Sciences, State University of New York, Albany, New York, USA. [3]Department of Atmospheric and Oceanic Sciences, University of California, Los Angeles (UCLA), California, USA. [4]Department of Atmospheric and Oceanic Sciences, University of Colorado at Boulder, Boulder, Colorado, USA. [5]Department of Physics, University of Helsinki, Helsinki, Finland. [6]National Center for Atmospheric Research, Boulder, Colorado, USA. [7]Pacific Northwest National Laboratory, Richland, Washington, USA. [8]NOAA, Earth System Research Laboratory, Chemical Sciences Division, Boulder, Colorado, USA. [9]Cooperative Institute for Research in Environmental Sciences, University of Colorado at Boulder, Boulder, Colorado, USA. [10]Institute for Meteorology and Geophysics, University of Innsbruck, Innsbruck, Austria. [11]University of Eastern Finland, Kuopio, Finland. †Present address: Meteorologisches Institut, Ludwig-Maximilians-Universität München, Germany.
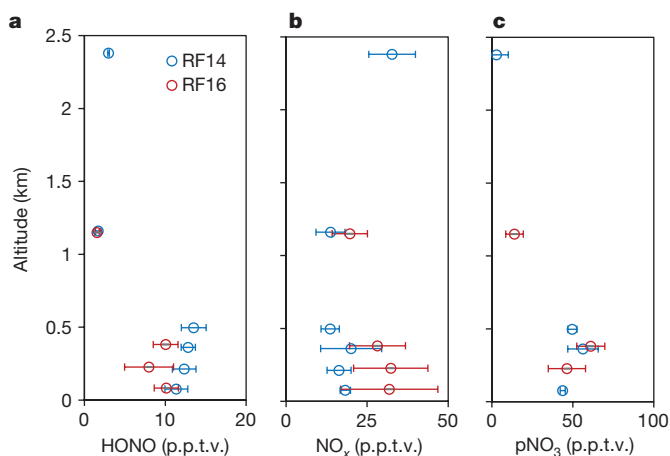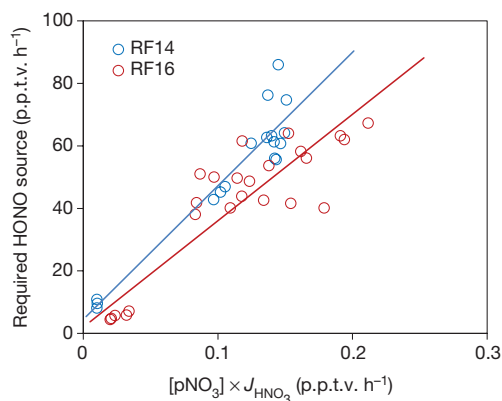
Figure 1 | Vertical profiles of HONO, NO_x and pNO_3 in marine air off the coast of North and South Carolina on 5 July 2013 (RF 14) and 8 July 2013 (RF 16). a, HONO; **b**, NO_x; **c**, pNO_3. Each error bar represents ±1 s.d. of the measurements. The height of the MBL is about 1 km.

Figure 2 | Correlation between the required *in situ* HONO source and the product of the pNO_3 concentration and the photolysis frequency of gaseous HNO_3. The lines are the linear least-squares fits to the data. The correlation coefficients (r^2) are 0.82 and 0.80 for RF14 and RF16, respectively. The relative uncertainty (±1 s.d.) is within 25% for the required *in situ* HONO source and within 35% for $J_{HNO_3} \times [pNO_3]$ in the MBL, and is within ~50% and ~70% in the free troposphere.

known HONO precursor, especially in urban environments[17]. However, there was no significant and positive correlation ($r^2 < 0.1$) between the concentrations of HONO and NO_x, suggesting that NO_x was not an important HONO precursor in the marine atmosphere. On the other hand, HONO and pNO_3 concentrations were much higher in the MBL than in the free troposphere (Fig. 1) and were significantly correlated ($r^2 = 0.62$ for RF14 and $r^2 = 0.61$ for RF16), suggesting that pNO_3 was a potential HONO precursor in the marine atmosphere. Indeed, the HONO source required to sustain the observed HONO concentration correlated well with the product of the pNO_3 concentration and HNO_3 photolysis frequency ($r^2 = 0.82$ for RF14 and $r^2 = 0.80$ for RF16) (Fig. 2). An enhancement factor of about 300 can be calculated from the slopes of linear least-squares fits for the photolysis rate constant of pNO_3 relative to that of gaseous HNO_3, if pNO_3 photolysis is the *in situ* HONO source sustaining the observed HONO concentrations after removing the minor contributions from NO_x-related reactions. A normalized photolysis rate constant for pNO_3, $J^N_{pNO_3}$, of ~$2.0 \times 10^{-4} s^{-1}$ can be derived from the enhancement factor, scaled to the typical tropical summer conditions on the ground (solar elevation angle $\theta = 0°$), corresponding to a gaseous HNO_3 photolysis rate constant of ~$7.0 \times 10^{-7} s^{-1}$ (refs 1 and 18).

To confirm the role of pNO_3 photolysis as a HONO source, aerosol samples were collected on board the C-130 aircraft using Teflon filters for the laboratory determination of the photolysis rate constants of pNO_3. A $J^N_{pNO_3}$ value of $1.0 \times 10^{-4} s^{-1}$ was determined from one aerosol sample collected during the MBL flight RF16. In addition, photolysis rate constants were determined to be in the range $1.3 \times 10^{-5} s^{-1}$ to $3.1 \times 10^{-4} s^{-1}$, with a median of $1.3 \times 10^{-4} s^{-1}$ and a mean ±1 s.d. of $(1.7 \pm 1.1) \times 10^{-4} s^{-1}$, from seven filter samples collected in various air masses during the NOMADSS flights, including one over the ocean (RF 16) and six over terrestrial environments in the southern and southeastern USA. HONO was the major product of pNO_3 photolysis under the experimental conditions, with an average HONO/NO_x production ratio of ~2. The laboratory-determined values are in reasonably good agreement with the value of ~$2.0 \times 10^{-4} s^{-1}$ inferred from the field observations (Fig. 2).

Both the field-inferred and the laboratory-determined $J^N_{pNO_3}$ values are also well within a reported range for the surface HNO_3 photolysis rate constant, from $2.2 \times 10^{-5} s^{-1}$ on glass surfaces[5,19] to $1.2 \times 10^{-3} s^{-1}$ on urban grime[6]. Similar to surface-adsorbed HNO_3, the high photolysis rate of pNO_3 may be due in part to its enhanced absorption cross-section, compared to that of gaseous HNO_3 (refs 7 and 8). The photolysis rate of pNO_3 associated with sea-salt aerosol may also be enhanced in the unique chemical environment of the MBL. Organic matter is ubiquitous and highly enriched in sea-salt

aerosols[20] and may serve as a photosensitizer for the photolysis of pNO_3. Furthermore, the relative humidity was measured to be mostly higher than the deliquescence point of sea-salt particles, and thus sea-salt particles were in the form of liquid droplets in the MBL. The light intensity is enhanced in sea-salt droplets owing to resonance and refraction[21], and the nitrate ion is attracted by Br^- to the air–water interface, where it becomes more photochemically reactive[22].

All the evidence from the field and the laboratory indicate that fast photolysis of pNO_3 in sea-salt aerosol sustains a majority of the observed HONO level in the MBL. Since HONO is readily photolysed to NO and OH during the day, the photolysis of pNO_3 becomes a 'renoxification' pathway. Sea-salt particles scavenge HNO_3 in the MBL, converting photochemically inert HNO_3 into photochemically reactive pNO_3 and thus accelerating the photochemical recycling of nitric acid/nitrate to NO_x in the MBL. Figure 3 shows diurnal cycling of the pNO_3–HONO–NO_x system, simulated by a box model based on the Master Chemical Mechanism (MCM v3.2)[10,11]. The observed and the predicted values during the early afternoon are in good agreement, within the measurement and model uncertainties. The simulated HONO and NO_x diurnal profiles were similar to those observed in the polar regions, where the photolysis of snowpack nitrate was the dominant HONO and NO_x source[23] and to that of NO_x in the clean MBL, where a photolytic NO_x source was proposed[24,25].

The predicted daytime HONO maximum is due to the strong HONO source from pNO_3 photolysis (Extended Data Fig. 2a). Other HONO sources included in our box model are the gas-phase reactions of OH with NO, of excited NO_2 with H_2O (refs 26 and 27), and of $HO_2 \cdot H_2O$ with NO_2 (refs 16 and 28), and heterogeneous reactions of NO_2 on sea-salt aerosol particles, but all of these have been found to be insignificant. The predicted daytime NO_x maximum is also due to the strong NO_x source from pNO_3 photolysis, partly though HONO as an intermediate (Extended Data Fig. 2b). Other known 'renoxification' processes in the gas phase, such as the HNO_3 + OH reaction and HNO_3 photolysis, are negligible NO_x sources in the clean MBL. NO_x is effectively oxidized to HNO_3 and pNO_3 via several mechanisms at comparable rates (Extended Data Fig. 2b). Of these mechanisms, the gas-phase reactions of NO_2 with OH and XO (X is primarily Br and I) are important HNO_3 and pNO_3 sources in the MBL[29]; the gas-phase reactions of NO with RO_2 radicals leading to organic nitrates have recently been reported to be the main sink of NO_x in low-NO_x forested environments[30]. The total nitrate (that is, HNO_3 + pNO_3) shows a net loss in the morning and a net gain from the mid-afternoon to early evening, with a balanced daily budget (Fig. 3). Model simulation results indicate that the pNO_3–NO_x cycling occurs on a scale of a few
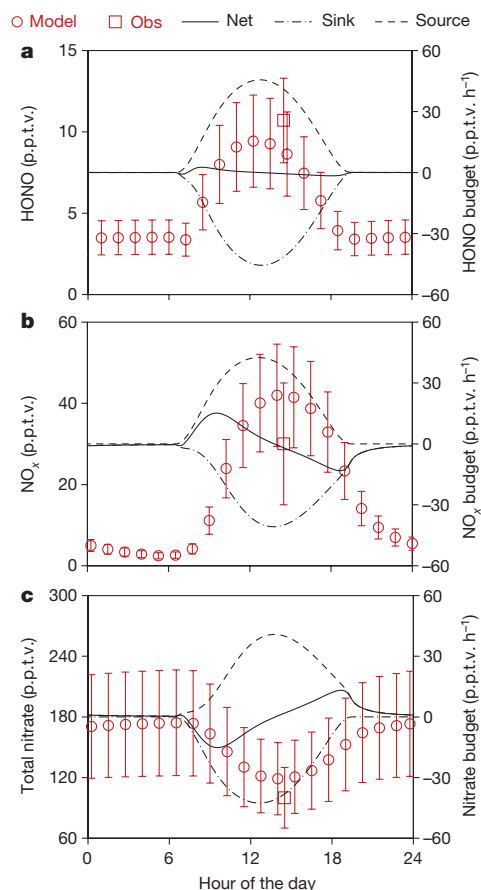
Figure 3 | Simulated diurnal profiles of mixing ratios and budgets for HONO, NO$_x$ and total nitrate in the MBL. a, HONO; **b**, NO$_x$; **c**, total nitrate (HNO$_3$+ pNO$_3$). HONO sources include reactions of excited NO$_2$ with H$_2$O (refs 26 and 27), of H$_2$O·HO$_2$ with NO$_2$ (refs 16 and 28), of OH with NO, the heterogeneous reaction of NO$_2$ on aerosols, and the photolysis of pNO$_3$. NO$_x$ sinks consist mainly of reactions of RO$_2$ with NO (ref. 30), of XO (primarily BrO and IO) with NO$_2$ (ref. 29) and of OH with NO$_2$. The error bar represents ±1 s.d. of the model calculations and field observations.

hours during the day, and is capable of sustaining the observed midday levels of HONO and NO$_x$ in the MBL.

The rapid pNO$_3$–HONO–NO$_x$ cycling suggests that the total nitrate in the troposphere is a NO$_x$ reservoir instead of the permanent NO$_x$ sink. The traditional view of the reactive nitrogen budget needs revision. Oceans account for over 70% of Earth's surface, so this recycling NO$_x$ could contribute substantially to the global NO$_x$ source. Moreover, this recycling source of NO$_x$ occurs in the MBL, where direct NO$_x$ emissions are negligible, and thus it could have profound impacts on global tropospheric chemistry, such as oxidant and secondary aerosol formation.

Online Content Methods, along with any additional Extended Data display items and Source Data, are available in the online version of the paper; references unique to these sections appear only in the online paper.

Received 14 July 2015; accepted 28 January 2016.
Published online 11 April 2016.

1. Finlayson-Pitts, B. J. & Pitts, J. N., Jr. *Chemistry of the Upper and Lower Atmosphere: Theory, Experiments and Applications* (Academic, 2000).
2. Wang, K., Zhang, Y., Nenes, A. & Fountoukis, C. Implementation of dust emission and chemistry into the Community Multiscale Air Quality modeling system and initial application to an Asian dust storm episode. *Atmos. Chem. Phys.* **12,** 10209–10237 (2012).
3. Deng, J., Wang, T., Liu, L. & Jiang, F. Modeling heterogeneous chemical processes on aerosol surface. *Particuology* **8,** 308–318 (2010).
4. Kumar, R. *et al.* Effects of dust aerosols on tropospheric chemistry during a typical pre-monsoon season dust storm in northern India. *Atmos. Chem. Phys.* **14,** 6813–6834 (2014).
5. Zhou, X. *et al.* Nitric acid photolysis on surfaces in low-NO$_x$ environments: significant atmospheric implications. *Geophys. Res. Lett.* **30,** 2217 (2003).
6. Baergen, A. M. & Donaldson, D. J. Photochemical renoxification of nitric acid on real urban grime. *Environ. Sci. Technol.* **47,** 815–820 (2013).
7. Zhu, C., Xiang, B., Chu, L. T. & Zhu, L. 308 nm photolysis of nitric acid in the gas phase, on aluminum surfaces, and on ice films. *J. Phys. Chem. A* **114,** 2561–2568 (2010).
8. Du, J. & Zhu, L. Quantification of the absorption cross sections of surface-adsorbed nitric acid in the 335–365 nm region by Brewster angle cavity ring-down spectroscopy. *Chem. Phys. Lett.* **511,** 213–218 (2011).
9. Zhou, X. *et al.* Nitric acid photolysis on forest canopy surface as a source for tropospheric nitrous acid. *Nature Geosci.* **4,** 440–443 (2011).
10. Saunders, S. M., Jenkin, M. E., Derwent, R. G. & Pilling, M. J. Protocol for the development of the Master Chemical Mechanism, MCM v3 (part A): tropospheric degradation of non-aromatic volatile organic compounds. *Atmos. Chem. Phys.* **3,** 161–180 (2003).
11. Jenkin, M. E., Saunders, S. M., Wagner, V. & Pilling, M. J. Protocol for the development of the Master Chemical Mechanism, MCM v3 (part B): tropospheric degradation of aromatic volatile organic compounds. *Atmos. Chem. Phys.* **3,** 181–193 (2003).
12. Ren, X. *et al.* OH, HO$_2$, and OH reactivity during the PMTACS–NY Whiteface Mountain 2002 campaign: observations and model comparison. *J. Geophys. Res.* **111,** D10S03 (2006).
13. Czader, B. H. *et al.* Modeling nitrous acid and its impact on ozone and hydroxyl radical during the Texas Air Quality Study 2006. *Atmos. Chem. Phys.* **12,** 6939–6951 (2012).
14. Lee, J. D. *et al.* Year-round measurements of nitrogen oxides and ozone in the tropical North Atlantic marine boundary layer. *J. Geophys. Res.* **114,** D21302 (2009).
15. Zhang, N. *et al.* Aircraft measurement of HONO vertical profiles over a forested region. *Geophys. Res. Lett.* **36,** L15820 (2009).
16. Li, X. *et al.* Missing gas-phase source of HONO inferred from Zeppelin measurements in the troposphere. *Science* **344,** 292–296 (2014).
17. Kleffmann, J. Daytime sources of nitrous acid (HONO) in the atmospheric boundary layer. *ChemPhysChem* **8,** 1137–1144 (2007).
18. Jankowski, J. J., Kieber, D. J., Mopper, K. & Neale, P. J. Development and intercalibration of ultraviolet solar actinometers. *Photochem. Photobiol.* **71,** 431–440 (2000).
19. Ramazan, K. A., Syomin, D. & Finlayson-Pitts, B. J. The photochemical production of HONO during the heterogeneous hydrolysis of NO$_2$. *Phys. Chem. Chem. Phys.* **6,** 3836–3843 (2004).
20. Turekian, V. C., Macko, S. A. & Keene, W. C. Concentrations, isotopic compositions, and sources of size-resolved, particulate organic carbon and oxalate in near-surface marine air at Bermuda during spring. *J. Geophys. Res.* **108** (D5), 4157 (2003).
21. Nissenson, P., Knox, C. J. H., Finlayson-Pitts, B. J., Philips, L. F. & Dabdub, D. Enhanced photolysis in aerosols: evidence for important surface effects. *Phys. Chem. Chem. Phys.* **8,** 4700–4710 (2006).
22. Richards, N. K. *et al.* Nitrate ion photolysis in thin water films in the presence of bromide ions. *J. Phys. Chem. A* **115,** 5810–5821 (2011).
23. Zhou, X. *et al.* Snowpack photochemical production of HONO: a major source of OH in the Arctic boundary layer in springtime. *Geophys. Res. Lett.* **28,** 4087–4090 (2001).
24. Val Martin, M., Honrath, R. E., Owen, R. C. & Li, Q. B. Seasonal variation of nitrogen oxides in the central North Atlantic lower free troposphere. *J. Geophys. Res.* **113,** D17307 (2008).
25. Helas, G. & Warneck, P. Background NO$_x$ mixing ratios in air masses over the North Atlantic Ocean. *J. Geophys. Res.* **86** (C8), 7283–7290 (1981).
26. Li, S., Matthews, J. & Sinha, A. Atmospheric hydroxyl radical production from electronically excited NO$_2$ and H$_2$O. *Science* **319,** 1657–1660 (2008).
27. Carr, S., Heard, D. E. & Blitz, M. A. Comment on "Atmospheric hydroxyl radical production from electronically excited NO$_2$ and H$_2$O". *Science* **324,** 336b (2009).
28. Ye, C. *et al.* Comment on "Missing gas-phase source of HONO inferred from Zeppelin measurements in the troposphere". *Science* **326,** 1657–1659 (2015).
29. Savarino, J. *et al.* Isotopic composition of atmospheric nitrate in a tropical marine boundary layer. *Proc. Natl Acad. Sci. USA* **110,** 17668–17673 (2013).
30. Browne, E. C. *et al.* Observations of total RONO$_2$ over the boreal forest: NO$_x$ sinks and HNO$_3$ sources. *Atmos. Chem. Phys.* **13,** 4543–4562 (2013).

Author Contributions Ye, C. and Zhou, X. designed and performed the field and laboratory studies, interpreted the data and write the manuscript with inputs from all the co-authors; Cantrell, C. and Ye, C. performed model simulations.

Author Information The data are available in our project data archive (http://data.eol.ucar.edu/master_list/?project=SAS). Reprints and permissions information is available at www.nature.com/reprints. The authors declare no competing financial interests. Readers are welcome to comment on the online version of the paper. Correspondence and requests for materials should be addressed to X.Z. (xianliang.zhou@health.ny.gov).

METHODS

Field measurements. Measurements on board the C-130 aircraft during the NOMADSS field campaign included HONO, pNO_3, NO_x, O_3, BrO, IO, OH radicals, HO_2 radicals, RO_2 radicals, aerosol surface area densities (for particle diameter <1 μm), VOCs, photolysis frequencies, and other meteorology parameters. Extended Data Table 1 summarizes the instrumentation, time resolution, detection limit, accuracy and references[31–40] for our measurements.

HONO was measured by two long-path absorption photometric (LPAP) systems based on the Griess–Saltzman reaction[31]. Briefly, ambient HONO was scrubbed by deionized water in a 10-turn glass coil sampler. The scrubbed nitrite was then derivatized with 5 mM sulfanilamide (SA) and 0.5 mM N-(1-naphthyl)-ethylene-diamine (NED) in 40 mM HCl, to form an azo dye within 5 min. The azo dye was detected by light absorbance at 540 nm using a fibre optic spectrometer (LEDSPEC-4, World Precision Instruments) with a 1-m liquid waveguide capillary flow cell (World Precision Instruments). 'Zero-HONO' air was generated by pulling ambient air through a Na_2CO_3-coated denuder to remove HONO and was sampled by the systems periodically to establish measurement baselines. Interference from NO_x, peroxyacetyl nitrate (PAN) and particulate nitrite, if any, was corrected by subtracting the baseline from the ambient air signal. Owing to the low collection efficiency of these interfering species in the sampling coil and their low concentrations, the combined interference signal was estimated to be less than 10% of the total signal in the clean MBL. Potential interference from peroxynitric acid (HO_2NO_2) was suppressed by heating the Teflon perfluoro-alkoxy alkanes (PFA) sampling line to 50 °C with a residence time of 0.8 s. The HO_2NO_2 steady-state concentration in the MBL was estimated to be less than 1 p.p.t.v. at a temperature of 23–26 °C in both flights, and thus interference from HO_2NO_2 was negligible[41]. Overall, the instrument baseline in the clean MBL was stable and low, and clear and strong ambient air signals (approximately ten times the detection limit) were observed. The accuracy of HONO measurements was confirmed by comparison with limb-scanning differential optical absorption spectroscopy (DOAS)[36]. The agreement between these two instruments was very good in wide power plant plumes, where HONO mixing ratios exceeded the lower detection limits of both instruments (Extended Data Fig. 3). HNO_3 and pNO_3 were quantitatively collected with a coil sampler and a fritted glass disk sampler, respectively. The collected nitrate in the two channels were reduced to nitrite by two cadmium (Cd) columns, and determined using two LPAP systems[31,32]. Zero air was generated to establish measurement baselines: for HNO_3 by passing the ambient air through a NaCl-coated denuder to remove HNO_3, and for pNO_3 through a Teflon filter and a NaCl-coated denuder to remove aerosol particles and HNO_3. Potential interference from HONO, NO_x and PAN was corrected by subtracting the baselines from the ambient air signals.

Ozone measurements were unavailable on 8 July 2013 and OH radical measurements were unavailable on 5 July 2013 owing to instrument malfunction. Steady-state OH radical concentrations were calculated and used in the budget analysis when OH radical measurements were not available[42]. Most of the parameters were observed at similar values during both flights, indicating that both flights captured the primary features of the local chemical environment. The lack of OH and O_3 measurements on the different flights had a negligible impact on our analysis. Several spikes in NO_x and aerosol surface area density detected from ship exhaust were excluded from the analysis.

Seventy-two-hour back-trajectories were calculated for both flights (Extended Data Fig. 1) with the Lagrangian particle dispersion model FLEXPART[43], version 9.02 (http://flexpart.eu), using six-hourly meteorological analysis data of the Global Forecasting System of the National Centers for Environmental Prediction (http://nomads.ncep.noaa.gov/txt_descriptions/GFS_half_degree_doc.shtml), interlaced with 3-h forecasts (0:00 UTC, 3:00 UTC, 6:00 UTC, 9:00 UTC, 12:00 UTC, 15:00 UTC, 18:00 UTC and 21:00 UTC), at a horizontal resolution of 0.5°. Every 5 min during the research flight 10,000 particles were released at the then-current position of the NSF/NCAR C-130 and followed back in time for 72 h. A 'particle' here refers to an infinitesimally small parcel of air, which is only affected by three-dimensional transport, turbulence and convection, and does not have any removal processes (no deposition, washout, sedimentation, chemical losses). Centroids shown in the figures are based on an algorithm[44] that reduces the residence probability distribution resulting from the locations of the 10,000 particles into five probable locations at each time interval.

Particulate nitrate photolysis experiment. One aerosol sample was collected using a Teflon filter (Sartorius, pore size 0.45 μm, diameter 47 mm) on-board the NSF/NCAR C-130 aircraft during every research flight from 30 min after take-off to 30 min before landing. The total sampling volume ranged from 1.1 m³ to 1.5 m³ depending on the flight length (ranging from 6 h to 8 h). The filter sample was wrapped in aluminium foil and stored in a refrigerator until use. The pNO_3 photolysis rate constant was determined using the filter sample in the laboratory.

The photochemical experiments were conducted using a cylindrical flow reactor (inner diameter 10 cm, depth 1.5 cm) with a quartz window on the top, at a

temperature of 21.0 ± 1.0 °C and a relative humidity of (50 ± 2)%. The filter sample was moved into the flow cell directly from the freezer for the photochemical experiment. Compressed air was purified by flowing through an activated charcoal and Purafil chemisorbant column (Purafil) to remove NO_x, VOCs, H_2S, SO_2, HNO_3 and HONO and was used as carrier gas. Gaseous products, HONO and NO_2, released during the experiment were flushed out of the reactor by the carrier gas, and were sampled by two coil samplers connected in series. The first 10-turn coil sampler scrubbed HONO with purified water at a collection efficiency of 100% (ref. 31), and the second 32-turn coil sampler was to scrub NO_2 with an acetic acid modified SA/NED solution at a collection efficiency of 60% (ref. 45). The scrubbed nitrite and NO_2 were converted to an azo dye with SA/NED reagents and analysed by two separate LPAP systems[31,45]. The filter sample was exposed to the solar simulator radiation for 10 min; baselines were established for both HONO and NO_2 before and after the light exposure. Photochemical production rates of HONO and NO_2 were calculated from their time-integrated signals above the baselines over the period of light exposure. To correct for HONO and NO_2 production from photolysis of HNO_3 deposited on the flow reactor wall surface, a control experiment was conducted by irradiating the empty flow reactor. The control signals were subtracted from the sample exposure signals when calculating the production rates of HONO and NO_2 from pNO_3 photolysis. After 10 min of light exposure, nitrate in the filter sample was extracted with 15 ml 1% NH_4Cl buffer solution (pH = 8.5), reduced to nitrite by a Cd column and determined by LPAP. A 300-W Ceramic xenon arc lamp (Perkin Elmer, model PE300BUV) was used as a light source. The ultraviolet light below 290 nm and the heat-generating infrared light were removed by a Pyrex glass filter and a water filter, respectively. The parabolic light beam irradiated only a circular area of a 1-inch (2.54 cm) diameter in the centre of the flow reactor. The shape of the spectrum of the filtered light source is similar to that of the solar actinic spectrum in the MBL (Extended Data Fig. 4). The effective light intensity in the centre of the flow reactor under direct irradiation was measured to be about 3.5 times higher than that at tropical noon on the ground (solar elevation angle θ = 0°)[1,18], using a nitrate actinometer[18]. The production rates of HONO and NO_2 were normalized by the amount of pNO_3 exposed and the effective ultraviolet light intensity, to obtain the normalized photolysis rate constants of pNO_3, $J^N_{pNO_3}$ (ref. 5).

$$J^N_{pNO_3} = \frac{P_{HONO} + P_{NO_2}}{N_{nitrate}} \times \frac{J_{nitrate,\,0°}}{J_{nitrate}} \qquad (1)$$

where P_{HONO} and P_{NO_2} are the production rates of HONO and NO_2, respectively; $N_{nitrate}$ is the light-exposed pNO_3 amount determined in the extraction solution; $J_{nitrate}$ is the photolysis rate constant of nitrate in the actinometer solution exposed to the experimental light source; and the 'standard' photolysis rate constant of aqueous nitrate ($J_{nitrate,0°} \approx 3.0 \times 10^{-7}\,s^{-1}$) is assumed for typical tropical summer conditions on the ground (solar elevation angle θ = 0°)[1,18], corresponding to a gas-phase HNO_3 photolysis rate constant ($J_{HNO_3,\,0°}$) of ~$7.0 \times 10^{-7}\,s^{-1}$. HONO is the major product from pNO_3 photolysis, with an average production ratio of HONO to NO_2 of 2.0. It should be noted that the $J^N_{pNO_3}$ value is calculated from the production rates of HONO and NO_2, and thus it may underestimate the photolysis rate constant of pNO_3 if other products, such as NO, are produced. However, NO was only a minor secondary product from the photolysis of HONO and NO_2, and accounted for ~1% of the total production of HONO and NO_2 in the flow reactor in a resident time of 8 s. Therefore, lack of NO measurement in this study would not affect the $J^N_{pNO_3}$ measurement. The overall uncertainty in the photolysis rate constant measurement is about 50%, taking into account the measurement uncertainties in production rates of HONO and NO_2, nitrate loading and effective ultraviolet light intensity.

It should be pointed out that the laboratory-determined $J^N_{pNO_3}$ represents merely an average photolysis rate constant of pNO_3 collected during the entire flight covering a wide geographic area, and thus does not reflect the possible temporal and spatial variability in the actual $J^N_{pNO_3}$ during the flight. In addition, the photochemical reactivity of bulk aerosol sample collected on the filter may be altered during sampling and handling, and thus the laboratory-determined $J^N_{pNO_3}$ using the bulk aerosol sample might be different from that under the ambient conditions. Nevertheless, the laboratory-determined $J^N_{pNO_3}$ is still the first and best estimate of the pNO_3 photolysis rate constant in the ambient atmosphere so far, and is in reasonable agreement with the values inferred from field observations (Fig. 2).

To evaluate the global recycling NO_x source from particulate nitrate photolysis, more aerosol samples need to be collected from different atmospheric environments all over the world, and better-designed experiments need to be conducted using these samples to more accurately determine the photolysis rates constants of particulate nitrate under conditions similar to those of ambient atmosphere.

Model simulations. The air masses encountered consisted mostly of aged air masses circulating within the boundary layer of the North Atlantic Ocean under a Bermuda high-pressure system for several days before reaching the measurement

locations (Extended Data Fig. 1). Within this relatively isolated air mass in the MBL, the cycling of pNO_3–HONO–NO_x was occurring much more rapidly, of the order of hours during the day, than dry deposition, which was of the order of days. Therefore, the diurnal chemistry of pNO_3–HONO–NO_x in the MBL can be simulated by a zero-dimensional box model.

Model simulations were conducted using the MCM v3.2 updated with the Jet Propulsion Laboratory's latest recommended kinetics[10,11,46], and constrained by the field-measured long-lived species, such as O_3, VOCs and total NO_y. The model was initiated from 00:00 local time and was allowed to run for three diurnal cycles (72 h). The diurnal concentration profiles of short-lived species, including OH, HO_2, HONO and NO_x, were affected by their initial concentrations only during the first diurnal cycle of simulation. The results presented here (Fig. 3, Extended Data Figs 2 and 5) were from the second diurnal cycle of the simulation run. To simulate the time-varying cycling of pNO_3–HONO–NO_x, the diurnal profiles of photolysis frequencies were also calculated by the MCM v3.2 and scaled by the measured values in the early afternoon. The time-dependent photolysis rate constant of particulate nitrate (J_{pNO_3}) at certain times of the day was calculated as follows:

$$J_{pNO_3} = J^N_{pNO_3} \times \frac{J_{HNO_3}}{J_{HNO_3,\,0°}} \tag{2}$$

where J_{HNO_3} is the photolysis rate constant of gas-phase HNO_3 measured in the MBL. The ratio of pNO_3 to HNO_3 was set to 1, as observed in the MBL during the early afternoon.

The photolysis of pNO_3 is considered a source of both HONO and NO_x. To include all the possible HONO sources in the model, the following reactions are also considered: the gas-phase reactions of OH with NO, of excited NO_2 with H_2O (refs 26 and 27), and of $HO_2\cdot H_2O$ with NO_2 (refs 16 and 28), and the heterogeneous reactions of NO_2 on sea-salt aerosol particles. Upper-limit HONO formation rates from reactions of excited NO_2 with H_2O and of $HO_2\cdot H_2O$ with NO_2 are calculated using the latest recommendations[27,28]. An upper-limit uptake coefficient of 10^{-4} was assumed for NO_2 uptake on sea-salt aerosol[47]. HONO sinks in the model include its photolysis and the gas-phase reaction with OH radicals.

The photolysis of pNO_3 is a NO_x source mainly through HONO as an intermediate. Other NO_x sources, such as the photolysis of gaseous HNO_3 and the reaction of gaseous HNO_3 with OH, are negligible, and are not included here. NO_x sinks include the formation of bromine nitrate ($BrONO_2$), iodine nitrate ($IONO_2$) and organic nitrate ($RONO_2$) as well as HNO_3 through the reactions of NO_2 with OH and of NO with HO_2. The uptake of halogen nitrate and organic nitrates on the sea-salt aerosols and following hydrolysis provide effective pathways for conversion of NO_x to particulate nitrate in addition to HNO_3 uptake. The photolysis lifetime of $BrONO_2$ in the gas phase was estimated to be ~12 min in the MBL, somewhat longer than the uptake and hydrolysis lifetime of ~6 min using an uptake coefficient of 0.8 on sea-salt aerosols[46]. Therefore, two-thirds of $BrONO_2$ is converted to pNO_3 through hydrolysis on the aerosol particle at midday. The photolysis lifetime of $IONO_2$ in the gas phase was estimated to be ~5 min (ref. 48), comparable to its uptake and hydrolysis lifetime[46,49]. Therefore, half of $IONO_2$ is converted to pNO_3 via hydrolysis on the aerosol particles at midday. BrO was measured at 1.5 p.p.t.v. by the DOAS instrument. The IO level was below the detection limit and was assumed to be at the typical MBL concentration[49,50] of 0.5 p.p.t.v.

To evaluate the impact of VOCs on reactive nitrogen chemistry, explicit methane chemistry is considered in the model. Higher VOCs are lumped into a single species, RH. The concentration of RH is adjusted by the sum of the abundance of individually measured VOCs (R_iH) scaled by the ratio of their rate coefficients for OH+R_iH to that for OH+CH_4. The products of OH+RH reactions lead to the formation of RO_2 radicals, carbonyls, peroxides, and organic nitrates. The yield of organic nitrate from the reaction of RO_2 radical with NO (reaction 3) is calculated based on the reaction rate of CH_3O_2 radical with NO ($k_{CH_3O_2+NO}$) and the effective branching ratio β.

$$RO_2 + NO \xrightarrow{\beta} RONO_2 \tag{3}$$

$$RO_2 + NO \xrightarrow{1-\beta} RO + NO_2 \tag{4}$$
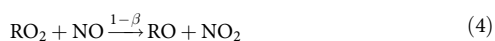
The effective branching ratio is calculated:

$$\beta = \frac{\sum k_i \beta_i [R_i O_2]}{k_{CH_3O_2+NO}[CH_3O_2]} \tag{5}$$

where $[R_iO_2]$ and $[CH_3O_2]$ are the concentrations of various R_iO_2 radicals formed from oxidation of various VOCs and methane, respectively; k_i and β_i are the recommended rate constants and branching ratios (β_i) for various RO_2 radicals, respectively[30,51]. The effective branching ratio β is estimated to be ~7% for our model. The fate of $RONO_2$ in the MBL is not well known; hydrolysis has been assumed to be an

effective sink of organic nitrates in forested regions[30]. In our model, an uptake coefficient of 10^{-2} and a 100% nitrate yield from $RONO_2$ uptake is assumed for organic nitrates on sea-salt aerosol.

The model is initialized with typically measured parameters and is run at 15-min time steps for three diurnal cycles. Multiple runs are used to constrain the model uncertainty by error propagation from the errors of all considered parameters. Gaussian error propagation is applied for the uncertainty calculation. Overall, a model uncertainty of 28% (± 1 s.d.) is calculated. The reactive nitrogen species are found to be reproducible for multiple days without considering deposition and transport. Sensitivity studies with the model indicate that the calculated HONO concentrations are relatively insensitive ($\leq 2\%$) to the following assumed parameters: the $RONO_2$ branching ratio (varying from 1% to 7% to 14%), the uptake coefficients of $RONO_2$ and $XONO_2$ (changing up and down by a factor of two), the nitrate yield from $RONO_2$ hydrolysis (varying from 5% to 100%), the initial concentration of non-methane hydrocarbons (changing up and down by a factor of two), and the RO_2+NO reaction rate constant (changing up and down by a factor of two). Changing up and down by a factor of two in the initial concentrations of BrO or IO leads to a change of up to 4% in the calculated HONO. Finally, the sensitivity of the model output to the ratio of HNO_3 to pNO_3 was assessed by varying between 0.5 and 2.0, and the modelled HONO varied between 1.17 and 0.74 of the value for the ratio of unity. Despite the simplicity of this model approach, the good agreement between model calculations and field observations for key species (Fig. 3 and Extended Data Fig. 5) shows its feasibility and usefulness for assessing the chemistry of radicals and reactive nitrogen in the MBL.

31. Zhang, N. et al. Measurements of ambient HONO concentrations and vertical HONO flux above a northern Michigan forest canopy. *Atmos. Chem. Phys.* **12,** 8285–8296 (2012).
32. Huang, G., Zhou, X., Deng, G., Qiao, H. & Civerolo, K. Measurements of atmospheric nitrous acid and nitric acid. *Atmos. Environ.* **36,** 2225–2235 (2002).
33. Ridley, B. et al. Florida thunderstorms: a faucet of reactive nitrogen to the upper troposphere. *J. Geophys. Res.* **109,** D17305 (2004).
34. Mauldin, R. et al. South Pole Antarctica observations and modeling results: new insights on HO_x radical and sulfur chemistry. *Atmos. Environ.* **44,** 572–581 (2010).
35. Hornbrook, R. S. et al. Measurements of tropospheric HO_2 and RO_2 by oxygen dilution modulation and chemical ionization mass spectrometry. *Atmos. Meas. Tech.* **4,** 735–756 (2011).
36. Platt, U. & Stutz, J. *Differential Optical Absorption Spectroscopy: Principles and Applications* (Springer, 2008).
37. Shetter, R. E., Cinquini, L., Lefer, B. L., Hall, S. R. & Madronich, S. Comparison of airborne measured and calculated spectral actinic flux and derived photolysis frequencies during the PEM Tropics B mission. *J. Geophys. Res.* **108** (D2), 8234 (2003).
38. Flagan, R. C. Electrical mobility methods for sub-micrometer particle characterization. In *Aerosol Measurement: Principles, Techniques, and Applications* 3rd edn (eds Kulkarni, P. Baron, P. A. & Willeke, K.), 339–364 (John Wiley & Sons, 2011).
39. de Gouw, J. & Warneke, C. Measurements of volatile organic compounds using proton-transfer-reaction mass spectrometry. *Mass Spectrom. Rev.* **26,** 223–257 (2007).
40. Hornbrook, R. S. et al. Observations of nonmethane organic compounds during ARCTAS—part 1: Biomass burning emissions and plume enhancements. *Atmos. Chem. Phys.* **11,** 11103–11130 (2011).
41. Gierczak, T., Jimenez, E., Riffault, V., Burkholder, J. B. & Ravishankara, A. R. Thermal decomposition of HO_2NO_2 (peroxynitric acid, PNA): rate coefficient and determination of the enthalpy of formation. *J. Phys. Chem. A* **109,** 586–596 (2005).
42. Cantrell, C. A. et al. Steady state free radical budgets and ozone photochemistry during TOPSE. *J. Geophys. Res.* **108** (D4), 8361 (2003).
43. Stohl, A., Forster, C., Frank, A., Seibert, P. & Wotawa, G. The Lagrangian particle dispersion model FLEXPART version 6.2. *Atmos. Chem. Phys.* **5,** 2461–2474 (2005).
44. Stohl, et al. A replacement for simple back trajectory calculations in the interpretation of atmospheric trace substance measurements. *Atmos. Environ.* **36,** 4635–4648 (2002).
45. Zhang, N. *Distributions and Sources of HONO in the Rural Troposphere.* PhD thesis, http://gradworks.umi.com/34/89/3489695.html (State Univ. New York, 2011).
46. Sander, S. et al. *Chemical Kinetics and Photochemical Data for Use in Atmospheric Studies, Evaluation No. 17* JPL Publication 10-6, http://jpldataeval.jpl.nasa.gov/pdf/JPL09_16Nov09_Sander.pdf (Jet Propulsion Laboratory, 2011).
47. Weis, D. D. & Ewing, G. E. The reaction of nitrogen dioxide with sea salt aerosol. *J. Phys. Chem. A* **103,** 4865–4873 (1999).
48. Joseph, D. M., Ashworth, S. H. & Plane, J. M. C. On the photochemistry of $IONO_2$: absorption cross section (240–370 nm) and photolysis product yields at 248 nm. *Phys. Chem. Chem. Phys.* **9,** 5599–5607 (2007).
49. McFiggans, G. et al. A modeling study of iodine chemistry in the marine boundary layer. *J. Geophys. Res.* **105** (D11), 14371–14385 (2000).
50. Dix, B. et al. Detection of iodine monoxide in the tropical free troposphere. *Proc. Natl Acad. Sci. USA* **110,** 2035–2040 (2013).
51. Zhang, J., Dransfield, T. & Donahue, N. M. On the mechanism for nitrate formation via the peroxy radical + NO reaction. *J. Phys. Chem. A* **108,** 9082–9095 (2004).
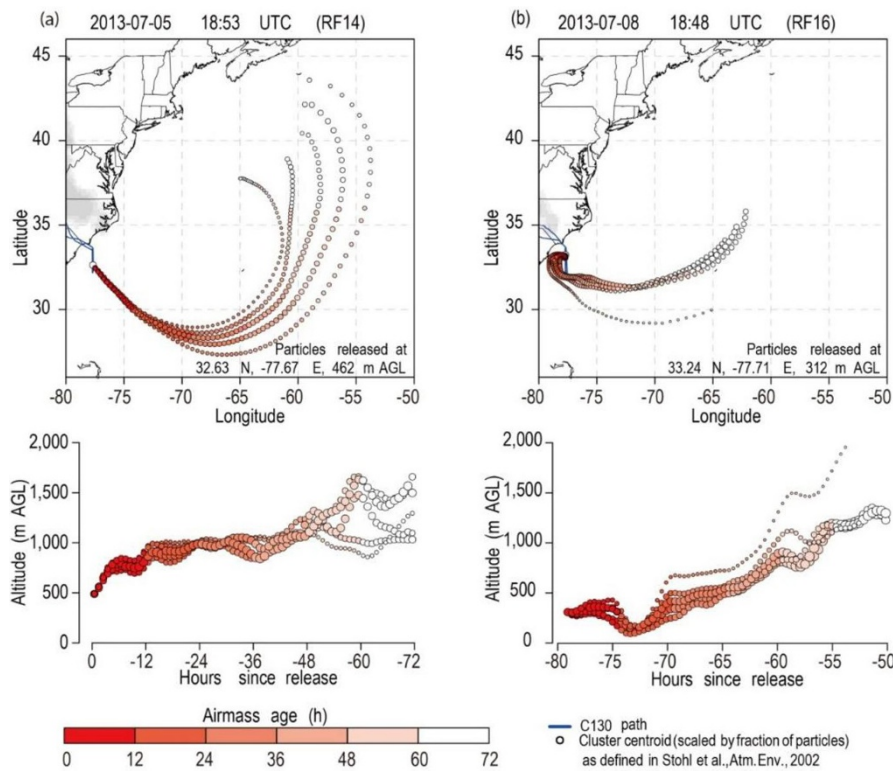
Extended Data Figure 1 | Typical back-trajectories of air masses in the MBL. a, 5 July 2013; **b**, 8 July 2013. The air mass circulated within the North Atlantic Ocean under a Bermuda high-pressure system for several days before reaching the measurement locations. On 8 July 2013, the air mass near the coast was also occasionally affected slightly by fresh emissions from the southeast coast of the USA. See ref. 44 for definition of the cluster centroid. The C-130 flight tracks are shown in upper panels by the lines from 33° 39′ N, 77° 42′ W to 32° 11′ N, 77° 41′ W over the North Atlantic Ocean. The altitudes of cluster centroids in the lower panels are in metres above ground level (AGL).
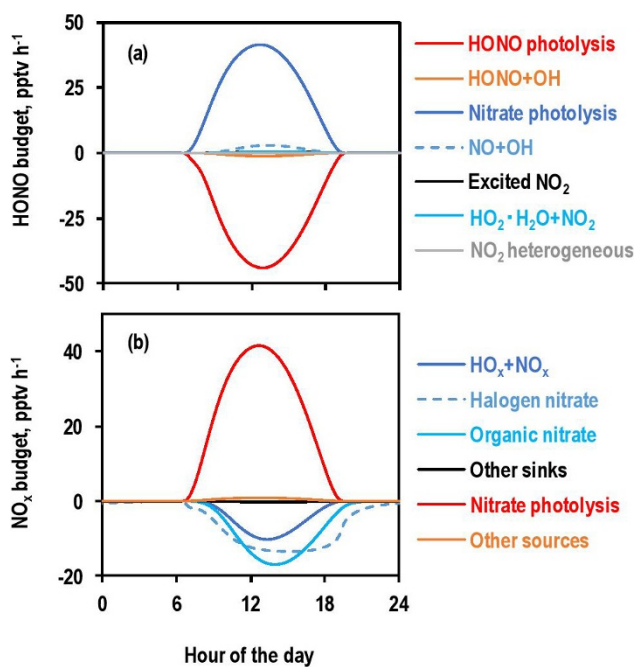
Extended Data Figure 2 | Typical diurnal HONO and NO$_x$ budgets in the clean MBL calculated by the MCM v3.2. a, HONO budget; **b**, NO$_x$ budget. 'HONO photolysis' and 'HONO+OH' represent HONO sinks contributed by HONO photolysis and the gas-phase reactions of HONO with the OH radicals. 'Nitrate photolysis', 'NO+OH', 'Excited NO$_2$', 'HO$_2$·H$_2$O+NO$_2$' and 'NO$_2$ heterogeneous' represent HONO sources contributed by pNO$_3$ photolysis, the gas-phase reactions of NO with OH, of excited NO$_2$ with H$_2$O and of HO$_2$·H$_2$O with NO$_2$, and the heterogeneous reactions of NO$_2$ on sea-salt aerosol particles, respectively. 'HO$_x$+NO$_x$' is the NO$_x$ sink contributed by gas-phase reactions of NO$_2$ with OH and of NO with HO$_2$ with a branching ratio of 0.5% (ref. 46). 'Halogen nitrate' is the NO$_x$ sink contributed by gas-phase reactions of NO$_2$ with primarily BrO and IO (ref. 29). 'Organic nitrate' is the NO$_x$ sink contributed by reactions of RO$_2$ radicals with NO with an effective branching ratio of 7% (refs 30 and 51). 'Other sinks' represents other minor NO$_x$ sinks, such as hydrolysis of N$_2$O$_5$. 'Nitrate photolysis' is the NO$_x$ source contributed by pNO$_3$ photolysis and 'Other sources' represents other minor NO$_x$ sources, such as photolysis of gaseous HNO$_3$.
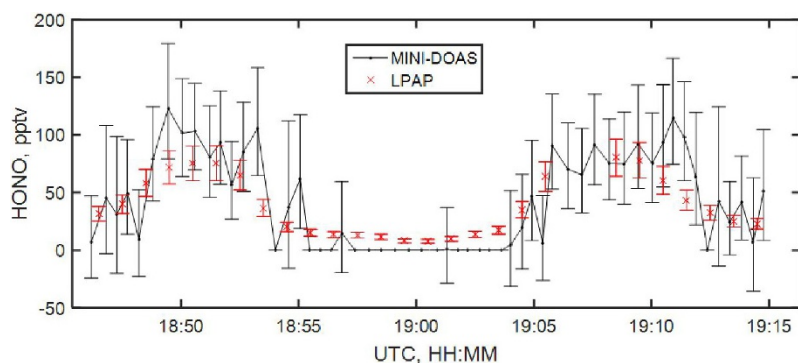
Extended Data Figure 3 | HONO observation comparison between the UCLA Mini-DOAS instrument and the LPAP instrument within two plumes during the research flight on 20 June 2013. The Mini-DOAS instrument is a limb-scanning Max-DOAS instrument, and the analysis incorporates the DOAS approach[36]. The differential slant column densities of HONO were scaled to the differential slant column density analysis of HCHO, which were retrieved in the same spectral interval and multiplied by the *in situ* HCHO measurements, provided by the TOGA instrument[40] to derive HONO mixing ratios. The Mini-DOAS data was obtained along various elevation viewing angles from +45° to −10°. Because of the position of the aircraft relative to the plumes, the plume geometry, and the HCHO scaling, the derived HONO mixing ratios do not depend on elevation viewing angle and this information was therefore omitted from the figure. Error bars (±1 s.d.) accompany each DOAS measurement. DOAS measurements influenced by clouds or aircraft manoeuvres have been removed from the figure. For better visibility negative DOAS values, which were statistically indistinguishable from zero, were set to 0 p.p.t.v. and the error bar was removed. Red error bars show a 20% uncertainty (±1 s.d.) for LPAP HONO results.
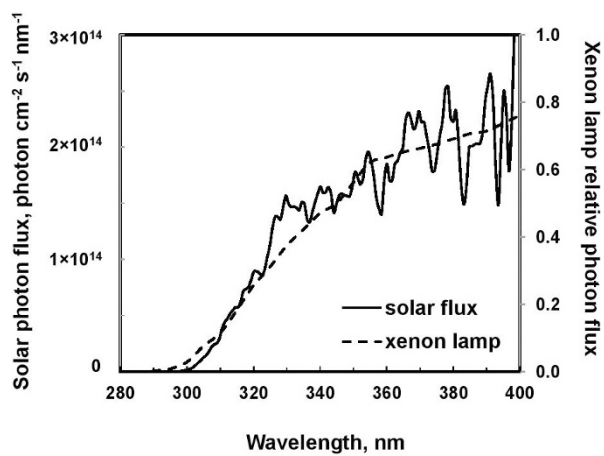
Extended Data Figure 4 | Comparison of the xenon arc lamp light spectrum with the solar actinic spectrum. The xenon light source was filtered by a 4-mm 7740 Pyrex filter, and the solar actinic flux was the 10-min measurement data at 360 m above sea level from 18:55 to 19:05 UTC during RF14.
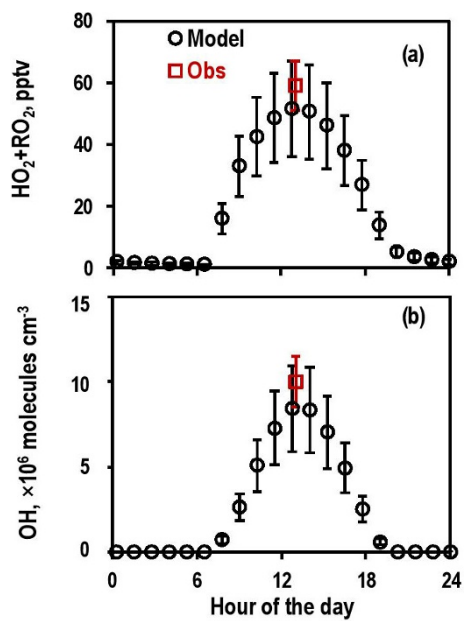
Extended Data Figure 5 | Typical diurnal profiles of HO_2+RO_2 and OH radicals in the clean MBL as observed and calculated by the MCM v3.2. a, HO_2+RO_2 radicals; **b**, OH radicals. The calculated (Model) and measured (Obs) ratio of HO_2 radicals to RO_2 radicals (CH_3O_2 plus higher RO_2) is about 1. The error bars represent ± 1 s.d. of the model calculations and observations.

Extended Data Table 1 | Measurements from the NOMADSS study used in this analysis

Parameters	Instrument	Time Resolution	Detection Limit	Accuracy	Reference
HONO	LPAP	200 s	1 pptv	20%	(31)
pNO_3	LPAP	360 s	5 pptv	30%	(31, 32)
HNO_3	LPAP	20 min	5 pptv	30%	(31, 32)
NO	CI	1 s	10 pptv	10%	(33)
NO_2	CI	1 s	20 pptv	15%	(33)
O_3	CI	1 s	100 pptv	5%	(33)
OH	SICIMS	30 s	$*5\times10^4$	30%	(34)
HO_2, RO_2	SICIMS	60 s	$*30\times10^6$	35%	(35)
BrO, IO	DOAS	60 s	1 pptv	20%	(36)
HONO	DOAS	60 s	~ 30 pptv	20%	(36)
Photolysis Frequencies	SAFS	1 s		18%	(37)
Surface area density	SMPS/UHSAS	65/1 s		20%	(38)
VOCs	PTRMS	15 s		20%	(39)
VOCs/organic nitrates	TOGA	120 s		20%	(40)

*In molecules per cm^3.

Data are from refs 31–40. CI, three-channel chemiluminescence instrument; SICIMS, selected-ion chemical-ionization mass spectrometer; SAFS, scanning actinic flux spectroradiometer; SMPS, scanning mobility particle sizer; UHSAS, ultrahigh-sensitivity aerosol spectrometer; TOGA, trace organic gas analyser; PTRMS, proton-transfer reaction mass spectrometry.